ISAR autofocus imaging algorithm for maneuvering targets based on deep learning and keystone transform

SHI Hongyin[*], LIU Yue, GUO Jianwen, and LIU Mingxin

School of Information Science and Engineering, Yanshan University, Qinhuangdao 066004, China

Abstract: The issue of small-angle maneuvering targets inverse synthetic aperture radar (ISAR) imaging has been successfully addressed by popular motion compensation algorithms. However, when the target's rotational velocity is sufficiently high during the dwell time of the radar, such compensation algorithms cannot obtain a high quality image. This paper proposes an ISAR imaging algorithm based on keystone transform and deep learning algorithm. The keystone transform is used to coarsely compensate for the target 's rotational motion and translational motion, and the deep learning algorithm is used to achieve a super-resolution image. The uniformly distributed point target data are used as the data set of the training u-net network. In addition, this method does not require estimating the motion parameters of the target, which simplifies the algorithm steps. Finally, several experiments are performed to demonstrate the effectiveness of the proposed algorithm.

Keywords: inverse synthetic aperture radar (ISAR), maneuvering target, keystone transform, deep learning, u-net network.

1. Introduction

Inverse synthetic aperture radar (ISAR) has been widely used for military and civilian purposes, such as target recognition, identification, and classification [1−5]. In general, real targets often have complex motion components [6,7]. These motion components lead to range distortion and Doppler frequency shift, which results in a defocused image. To obtain focused ISAR image, motion compensation is done in two steps. The first step is translational motion compensation, which consists of range alignment and phase adjustment [8,9]. The second step is rotational motion compensation.

In order to obtain an ideal ISAR image during imaging processing, the motion-compensated point scatterers are

required to stay in the initial distance unit, so that the image of the point scatterers will not appear in several distance units at the same time, resulting in defocusing [10,11]. However, in the actual ISAR imaging process, the phenomenon of movement around the point scatterer often occurs, especially in the high-resolution imaging. The possibility of range cell migration correction (RCMC) occurring at the scattering point will be greatly increased due to the improvement of the distance resolution [12]. However, RCMC has its own characteristics, which is caused by the coupling of its signal distance frequency domain and slow time domain. Keystone transform is widely used to correct the motion of the scatter point and the resolution element [13].

Deep learning has gained popularity and defined the state-of-the-art results in various fields in science and engineering; these include speech recognition, natural language understanding, visual object recognition, and many other applications [14−18]. Deep convolutional neural networks (CNNs) are first applied to image classification, and its output is the category of image [19,20]. However, the output of image segmentation is an image, so it can be regarded as classifying every pixel in the image. Based on this, Ronneberger et al. [21] proposed a u-net network structure in 2015, which can achieve the same resolution of input and output. Mccann et al. [22] applied this network to the inverse problem of medical imaging. Taking the blurred image generated by sparse signal as the input of the network and outputting the clear image from the full view, it is proved that the u-net network is effective for image super-resolution.

Based on that, this paper focuses on the imaging problem of large-angle targets, and proposes an ISAR imaging algorithm based on keystone transform and deep learning. This makes it possible to get a clear ISAR image when the target rotation angle is large.

The rest of the paper is organized as follows: maneuvering target echo signal analysis is shown in Section 2. In

Section 3, we focus on the theory of keystone transform and u-net network. Experimental simulation analysis is presented in Section 4, and conclusions are given in Section 5.

2. Maneuvering target imaging model

Fig. 1 shows the ISAR imaging geometry of a maneuvering target. It is assumed that P is a random point scatterer on the target in the far field of radar, and the target has rotational and translational motion in the radial direction. The target angular velocity is ω, the radial velocity is v_r, and the origin of the coordinate system is the center of rotation.
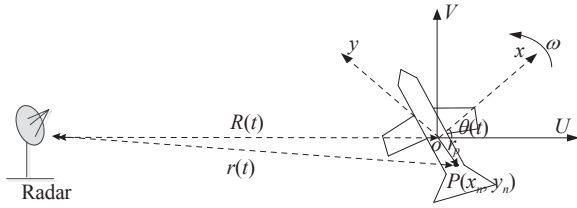

Fig. 1   ISAR imaging geometry model of a maneuvering target

Assume that the stepped-frequency continuous wave (SFCW) form signal transmitted by the radar has M bursts and N frequency steps, and it is described by a sequence of N pulses with increased carrier frequencies: $f_n = f_c + m\Delta f$ ($m = 0, 1, 2, \cdots, N-1$), where f_c is the carrier frequency, and Δf is the frequency step. The echoes of all point scatterers can be expressed as

$$s(t,m) = \sum_{k=1}^{K} A_k \exp\left\{-j\frac{4\pi}{c}(f_c + m\Delta f)r(t)\right\} \quad (1)$$

where A_k is the reflectivity density at point k, c is the speed of light, $r(t)$ is the distance from the radar to the point P:

$$r(t) = \left[R(t)^2 + r_P^2 + 2R(t)r_p \sin\theta(t)\right]^{\frac{1}{2}} \quad (2)$$

where $r_p = \sqrt{x_n^2 + y_n^2}$, (x_n, y_n) is any point on the target, $R(t)$ is the distance between the radar and the target, which can be expanded with Taylor series as

$$R(t) = R_0 + v_r t + \cdots \quad (3)$$

where R_0 is the initial distance of the radar to the target.

Taking the first two terms of the Taylor series, we have

$$R(t) = R_0 + v_r t. \quad (4)$$

Assuming the initial angle of the target is 0, the target rotation angle $\theta(t)$ can be expressed as

$$\theta(t) = \omega t. \quad (5)$$

Since R_0 is much larger than r_p, the distance between the points and the radar can be approximated as

$$r(t) \cong R(t) + x_n \cos(\omega t) - y_n \sin(\omega t). \quad (6)$$

Assume the coherent processing interval (CPI) is not too long, then we can get

$$\cos(\omega t) \cong 1 - \frac{1}{2}(\omega t)^2, \quad (7)$$

$$\sin(\omega t) \cong \omega t. \quad (8)$$

Thus, $r(t)$ can be written as

$$r(t) \cong R(t) + x_n - \frac{1}{2}x_n\omega^2 t^2 - y_n\omega t =$$

$$R_o + v_r t + x_n - \frac{1}{2}x_n\omega^2 t^2 - y_n\omega t. \quad (9)$$

Therefore, we can rewrite the base-band signal as

$$s(t,m) = \sum_{k=1}^{K} A_k \exp\left[-j\frac{4\pi}{c}(f_c + m\Delta f)\right]\cdot$$

$$\exp\left[R_0 + v_r t + x_n - \frac{1}{2}x_n\omega^2 t^2 - y_n\omega t\right] =$$

$$\sum_{k=1}^{K} A_k \exp\left[-j\frac{4\pi(m\Delta f + f_c)}{c}(R_0 + x_n)\right]\cdot$$

$$\exp\left[-j\frac{4\pi(m\Delta f)}{c}(v_r t)\right]\cdot$$

$$\exp\left[j\frac{4\pi(m\Delta f)}{c}\left(\frac{1}{2}x_n\omega^2 t^2 + y_n\omega t\right)\right]\cdot$$

$$\exp\left[-j\frac{4\pi f_c}{c}\left(v_r t - \frac{1}{2}x_n\omega^2 t^2 - y_n\omega t\right)\right]. \quad (10)$$

In (10), the first term is a constant, indicating the distance distribution of scattering points, which can be ignored in the imaging process. The second term represents the echo envelope movement caused by the translation motion. The third term represents the echo envelope movement caused by the rotation motion. The fourth term represents the carrier phase change caused by the Doppler effect. In the second and third terms, different slow times have different envelope translations. When the translation motion exceeds a range resolution unit, RCMC will be generated, and the scatterers drift from its original range position x_n to a new position $\left(R_0 + v_r t + x_n - \frac{1}{2}x_n\omega^2 t^2 - y_n\omega t\right)$, so it is necessary to remove such phase errors along the range-direction.

3. Algorithm theory and application

3.1   Keystone transform

From the radar echo data [23], the RCMC is expressed as the coupling between the signal frequency f and the slow time t. The virtual time τ is defined as

$$f_c\tau = (f + f_c)t. \tag{11}$$

Thus, (10) becomes

$$s(\tau,m) = \sum_{k=1}^{K} A_k \exp\left[-\mathrm{j}\frac{4\pi(m\Delta f + f_c)}{c}(R_0 + x_n)\right]\cdot$$
$$\exp\left[-\mathrm{j}\frac{4\pi}{c}(f_c v_r \tau - f_c y_n \omega \tau)\right]\cdot$$
$$\exp\left[-\mathrm{j}\frac{4\pi}{c}\left(-x_n\omega^2\frac{f_c^2\tau^2}{2(f+f_c)}\right)\right]. \tag{12}$$

Since f_c is much larger than $m\Delta f$, we have

$$s(\tau,m) = \sum_{k=1}^{K} A_k \exp\left[-\mathrm{j}\frac{4\pi(m\Delta f)}{c}(R_0 + x_n)\right]\cdot$$
$$\exp\left\{-\mathrm{j}\frac{4\pi f_c}{c}\left[v_r\tau - y_n\omega\tau - \frac{1}{2}x_n\omega^2\tau^2\right]\right\}. \tag{13}$$

After applying the keystone transform, f and t have been decoupled in the second term of the phase function. If we perform the inverse Fourier transform with respect to the fast-time index n, the quadratic term $-\frac{1}{2}x_n\omega^2\tau^2$ can be neglected compared with the actual size of the range resolution cell.

By differentiating the phase in (12), the Doppler frequency shift introduced by the carrier phase change can be calculated as

$$f_d \cong -\frac{2f_c}{c}(v_r - y_n\omega). \tag{14}$$

According to the above equation, in the coherent processing interval, the Doppler frequency shift changes linearly due to the existence of velocity, which will lead to the frequency dispersion of the echo signal and have a great impact on the distance resolution.

For the ISAR imaging system, the electromagnetic wave transmits through the space and back can be regarded as a complex nonlinear system between the target and the radar. In the 2-D field, we can describe the echo data $s(x,r)$ as

$$s(x,r) = \sigma(x,r)\otimes_i\otimes_x h(x,r) \tag{15}$$

where $\sigma(x,r)$ and $h(x,r)$ represent the backscatter coefficients of the target field and the impulse response functions of the radar system, respectively, and $\otimes$ is the convolution operation.

ISAR imaging is an inverse problem, which is to solve the function $\sigma(x,r)$ from the radar echo $s(x,t)$, it is the process of solving a two dimensional convolution, it can be expressed as

$$\hat{\sigma}(x,r) = s(x,r)\otimes_i\otimes_x h_s(x,r) \tag{16}$$

where $h_s(x,r)$ is the impulse response function of the imaging system. Theoretically, if we can design $h_s(x,r)$ to satisfy

$$h(x,r)\otimes h_s(x,r) = \delta(x,r) \tag{17}$$

where $\delta(\cdot)$ represents the impulse function, then $\hat{\sigma}(x,r)$ is the reconstruction of $\sigma(x,r)$ without distortion. However, due to the effects of complex movement on maneuvering targets, it is difficult to design an accurate non-linear function $h_s(x,r)$ to reconstruct the target image. In this paper, we use the non-linear function fitting ability of the CNN to realize image reconstruction.

3.2 CNN model

Considering that the original u-net training is slow, in this paper, we build a more elegant architecture fully convolutional network [24]. We modify and extend this architecture such that it works with very few training images and yields more precise segmentations, see Fig. 2. The main idea is to add a batch normalization (BN) layer behind each convolution layer. Normalized input features can speed up the learning process and make it easier to optimize the algorithm. This is normalization of the input layer. The extension of normalization to each layer is the core idea of the BN layer, that is, the output of the upper layer does not affect the training of this layer, so that each layer of data has its own distribution and speeds up the training process.
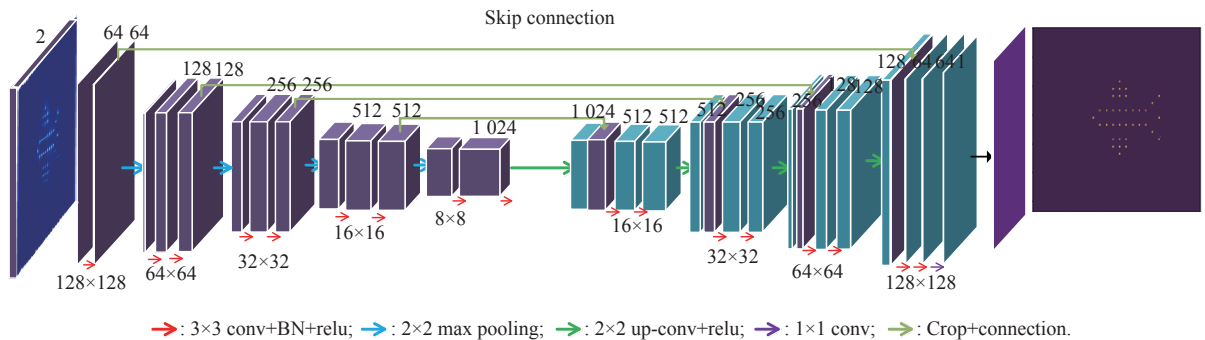

Fig. 2 Modified network structure of u-net

Firstly, the BN layer processing flow includes the following steps. Calculate the mean within the batch:

$$\mu = \frac{1}{\lambda} \cdot z^{[i]}. \tag{18}$$

Secondly, calculate the variance:

$$\xi = \sum (z^i - \xi)^2. \tag{19}$$

Thirdly, normalize z^i:

$$z_{\text{norm}}^i = \frac{z^i - \mu}{\sqrt{\xi^2 + \varepsilon}}. \tag{20}$$

Finally, adjust Z_i:

$$Z_i = \alpha \cdot z_{\text{norm}}^i + \beta \tag{21}$$

where α and β are the parameters of network learning and they are updated in reverse propagation.

The BN layer has two advantages. One is that each dimension of each layer is normalized, which can make the network have a higher learning rate, and the other is that it can slightly reduce the over-fitting effect.

The modified network structure is shown in Fig. 2.

Some modifications have been made to the network to enhance radar imaging. Firstly, because the radar echo signal is a complex signal, the following adjustments are made to the u-net input channel. The number of u-net input channels is changed to two. The real and imaginary data are put into two channels respectively, and the output dimension remains unchanged. Secondly, in a 3×3 convolution, the valid convolution mode is changed to sample convolution while keeping the size of the picture unchanged. Thirdly, considering the time and efficiency, the number of generated pulses is 128, the number of sampling points is 128, the input size is 128×128×2, and the output size is 128×128×1. Finally, in order to speed up the training of the network, the real part and imaginary part of the input complex image are normalized by the maximum and minimum values respectively:

$$\eta^* = \frac{\eta - \eta_{\min}}{\eta_{\max} - \eta_{\min}} \tag{22}$$

where η is the size of each pixel, $\eta_{\min}$ is the smallest pixel value in the image, and $\eta_{\max}$ is the largest pixel value in the image.

After normalization, the size of each pixel in the input image can be mapped to $[0, 1]$, which makes training easier.

3.3 Algorithm implementation flow

Fig. 3 shows the flow chart of the algorithm in this paper, point target coordinates are generated, and then echo data are obtained by (13). Since the rotation angle and velocity of the target are unknown, the output will be defo-

cused if it passes the network. Therefore, this paper firstly performs preprocessing by the motion compensation algorithm (keystone transform), which can compensate for the phase errors caused by the target's rotational motion and translational motion. Then, fast Fourier transform (FFT) is performed, and put the real and imaginary data into the network's prediction input.
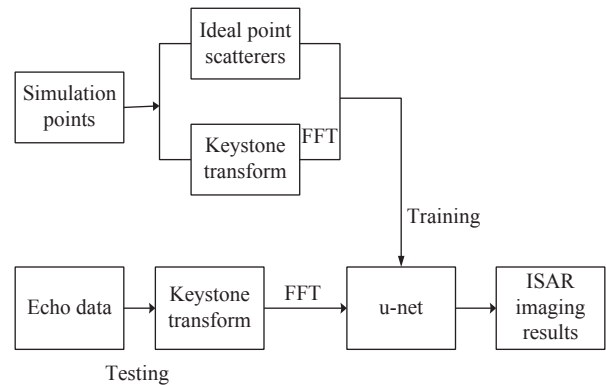

Fig. 3 Flow chart of the algorithm in this paper

The radar parameters are shown in Table 1.

Table 1 Radar imaging parameters

Radar parameter name	Symbol	Numerical value
Initial frequency of transmitted signal	f_0/GHz	3
Target initial distance	R_0/km	10
Pulse repetition frequency	PRF/KHz	50
Transmit signal bandwidth	B/MHz	150
Number of bursts	M_{burst}	128
Number of pulses	N_{pulse}	128

4. Simulation analysis

4.1 Training data generation

In this paper, in order to obtain better training results, the first quadrant points in the training set are uniformly distributed, and the other quadrant points are consistent with the first quadrant points. The points obtained are distributed in the four quadrants, and eventually 1 000 training data are obtained.

The FFT image varies with the motion parameters, so it cannot be trained and predicted by the neural network, but the image is relatively good by using keystone transform. Therefore, for the imaging of maneuvering targets, in the training, motion compensation is firstly carried out by keystone transform, which roughly compensates the additional phase generated by translation and rotation, and then the results are obtained by FFT, which is placed in the u-net network for training. In the training set of this paper, the rotational angular velocity of the target is

0.15 rad/s, the radial velocity of the target is 2 m/s, Fig. 4(a) is the FFT image, Fig. 4(b) is the imaging result after keystone transform, and Fig. 4(c) is the ideal point scatterers model.
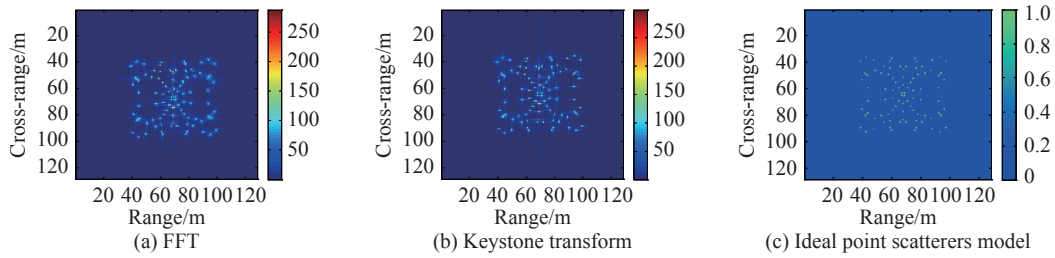

(a) FFT

(b) Keystone transform

(c) Ideal point scatterers model

Fig. 4   Training samples

4.2   Analysis of results

4.2.1   Experiment 1

Fig. 5 shows the ISAR images of different targets at a speed of 2 m/s and a rotation angle of 0.15 rad/s, and Fig. 5(a) and Fig. 5(e) are the FFT imaging results. It can be seen from the figure that the obvious defocusing phenomenon occurs due to the range cell migration caused by rotational and translational motions. Keystone transform can coarsely compensate for the target's rotational motion and translational motion, as shown in Fig. 5(b) and Fig. 5(f).

Fig. 5(c) and Fig. 5(g) are the u-net prediction results, and Fig. 5(d) and Fig. 5(h) show the ideal point scatterers model. The point scatterer used to analyze the profile is circled in red in the image. Fig. 6 shows the range and azimuth profile comparison. It can be seen that, under the FFT algorithm, there is no sidelobe in azimuth and range echo; under keystone transform, the azimuth peak sidelobe is good, but the range peak sidelobe is very high, while the deep learning algorithm greatly improves the sidelobe suppression performance and has a better focusing degree.
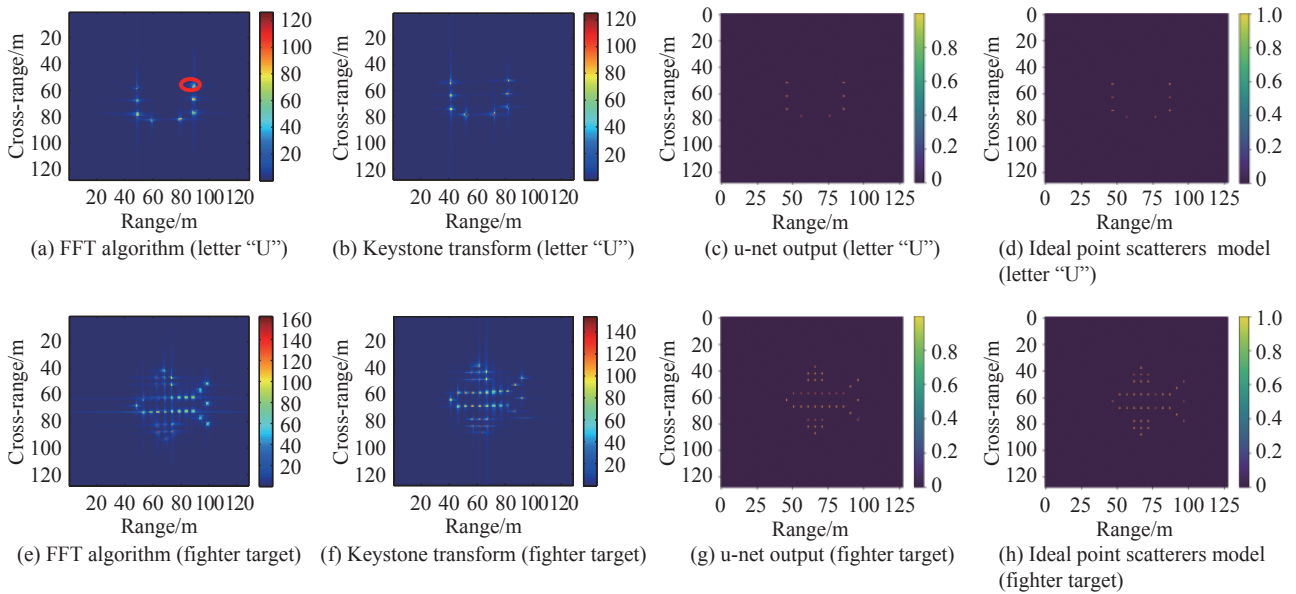

(a) FFT algorithm (letter "U")

(b) Keystone transform (letter "U")

(c) u-net output (letter "U")

(d) Ideal point scatterers model (letter "U")

(e) FFT algorithm (fighter target)

(f) Keystone transform (fighter target)

(g) u-net output (fighter target)

(h) Ideal point scatterers model (fighter target)

Fig. 5   Algorithm of this paper tests results for different targets

We compare the proposed algorithm with Gabor wavelet transform (GWT) and polar formatting algorithm (PFA). Fig. 7 shows the ISAR images of the maneuvering target at a speed of 2 m/s and a rotation angle of 0.15 rad/s, Fig. 7(a) is the GWT imaging result, and Fig. 7(b) is the PFA imaging result. It can be seen that after GWT and PFA preprocessing, due to the effect of the residual phase error after coarse compensation, the image is still defocused in the direction of distance and cross distance. Fig. 7(c) is the proposed method result, where the error phase is successfully removed and a clear ISAR image is formed. The point scatterer used to analyze the profile is circled in red in the image. Fig. 8 shows the range and azimuth profile comparison. It can be seen that the proposed method has the minimum peak to side lobe ratio and shows high performance in correction of phase error.
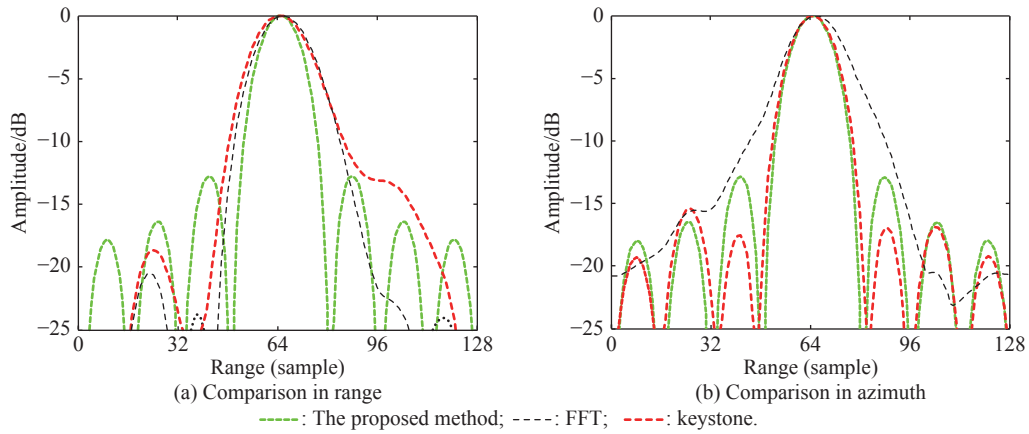
(a) Comparison in range

(b) Comparison in azimuth

----: The proposed method; -----: FFT; ----: keystone.

Fig. 6 Profile comparison of the point scatterer marked by the red circle in Fig. 5(a)

(a) GWT

(b) PFA

(c) u-net output
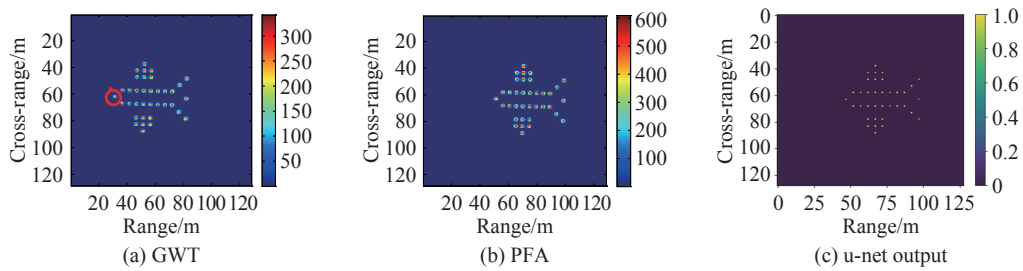
Fig. 7 Simulation results of different algorithms

(a) Comparison in range

(b) Comparison in azimuth

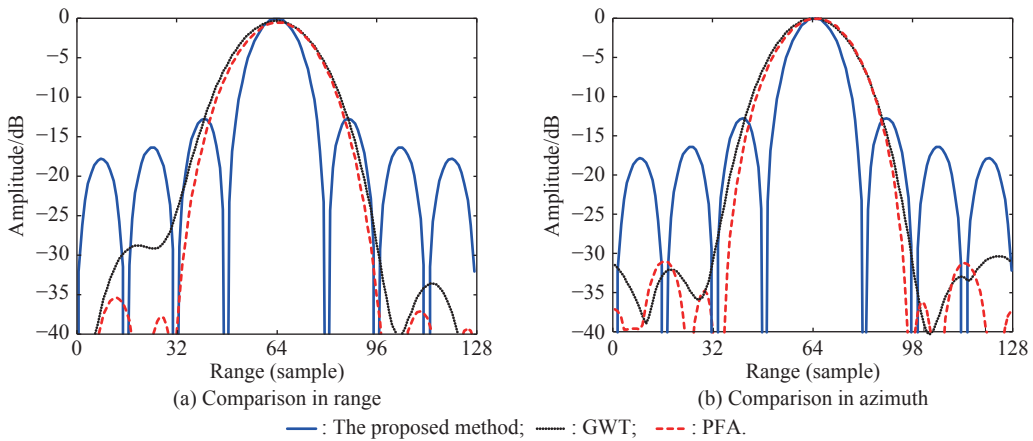——: The proposed method; ......: GWT; ----: PFA.

Fig. 8 Profile comparison of the point scatterer marked by the red circle in Fig. 7(a)

4.2.2 Experiment 2

In this paper, the measured data of Boeing 727 aircraft provided by the U.S. naval research laboratory are used for experimental simulation. Fig. 9 shows the ISAR images at a speed of 2 m/s and a rotation angle of 0.16 rad/s, and Fig. 10 shows the profile of the point scatterer on the tail of the aircraft marked by a red circle in Fig. 9(a).
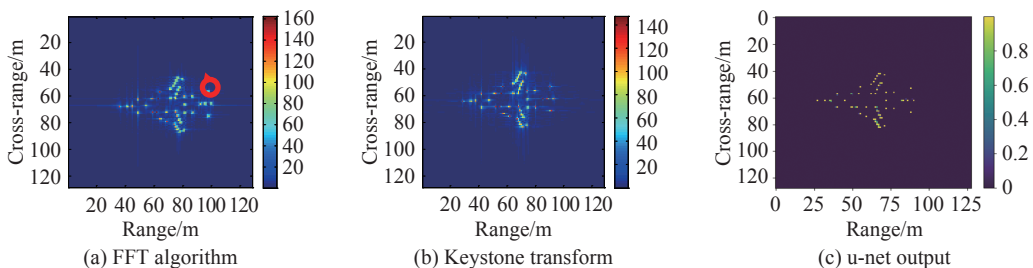

(a) FFT algorithm

(b) Keystone transform

(c) u-net output

Fig. 9 Simulation results of Boeing 727

(a) Comparison in range

(b) Comparison in azimuth

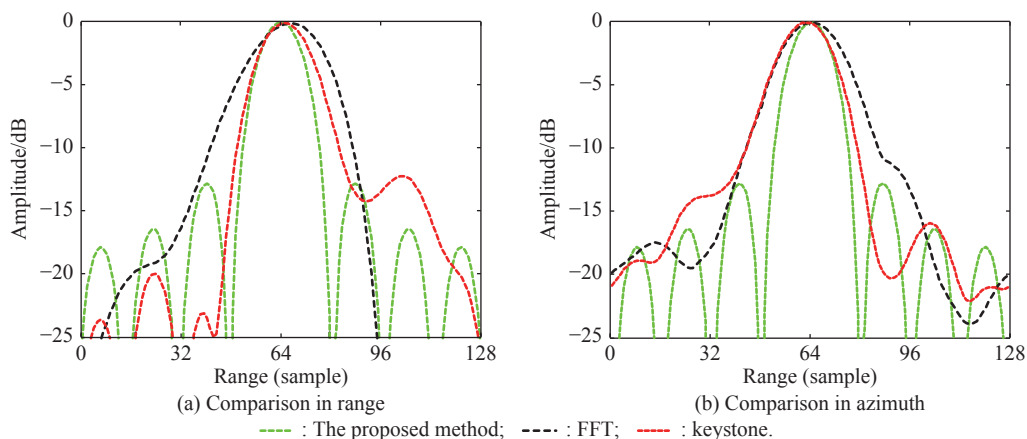---- : The proposed method;   ---- : FFT;   ---- : keystone.

Fig. 10   Profile comparison of the point scatterer marked by the red circle in Fig. 9(a)

Fig. 11 shows the ISAR images at a speed of 3 m/s and a rotation angle of 0.14 rad/s, and Fig. 12 shows the profile of the point scatterer on the tail of the aircraft marked by a red circle in Fig. 11(a). Compared to the FFT al-gorithm and the keystone transform, the proposed meth-od has a smaller peak sidelobe ratio, and it obtains a more focused image in both directions.
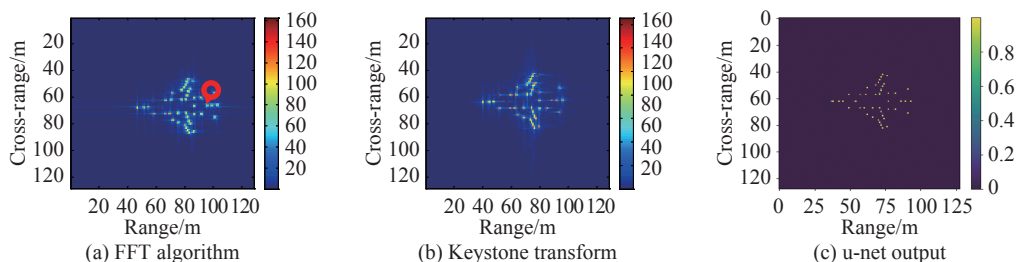

(a) FFT algorithm

(b) Keystone transform

(c) u-net output

Fig. 11   Simulation results of Boeing 727

(a) Comparison in range

(b) Comparison in azimuth

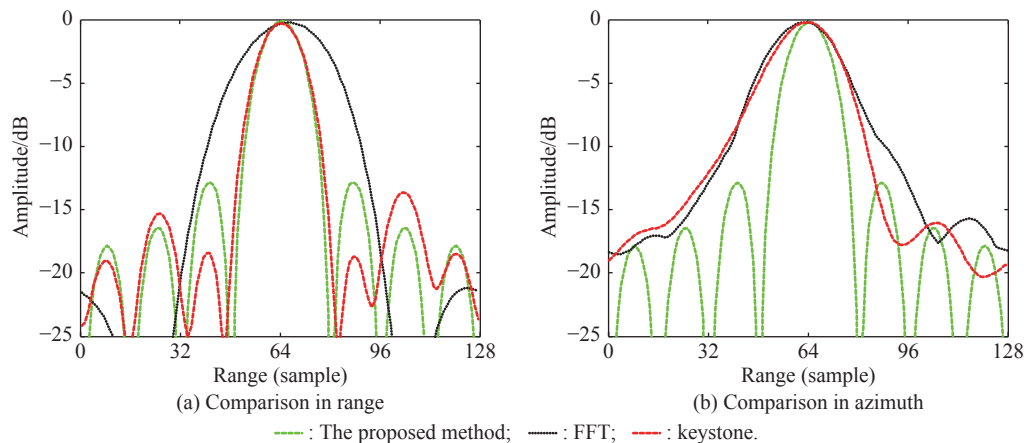---- : The proposed method;   ---- : FFT;   ---- : keystone.

Fig. 12   Profile comparison of the point scatterer marked by the red circle in Fig. 11(a)

From the above simulation results and analysis, it can be seen that the proposed method achieves high resolu-tion imaging of moving targets, and it only needs 0.56 s to realize fast imaging on TITAN BLACK GPU through network.

5. Conclusions

In this paper, an ISAR imaging algorithm based on key-stone transform and deep learning imaging is proposed for the moving target with large rotation angle and small speed. The keystone transform preprocesses echo data to roughly compensate the translation and rotation of the target, and then takes the uniformly distributed point tar-get data as the training dataset of u-net neural network to obtain 1 000 training set data. The u-net neural network is used to predict maneuvering targets in different motion situation and to obtain high resolution images. The ima-ging results verify the effectiveness of the method.

References

[1] BOERS Y, SALMOND D. Editorial-target tracking: algorithms and applications. IEE Proceedings —Radar, Sonar & Navigation, 2005, 152(5): 289–290.

[2] BENEDEK C, MARTORELLA M. ISAR image sequence based automatic target recognition by using a multi-frame marked point process model. Proc. of the International Geoscience and Remote Sensing Symposium, 2011: 3791–3794.

[3] SHI H Y, XIA S X, TIAN Y. ISAR imaging based on improved phase retrieval algorithm. Journal of Systems Engineering and Electronics, 2018, 29(2): 278–285.

[4] SHIN S, SHIN S Y, MYUNG N, et al. The application of motion compensation of ISAR image for a moving target in radar target recognition. Microwave & Optical Technology Letters, 2010, 50(6): 1673–1678.

[5] MARTORELLA M. Analysis of the robustness of bistatic inverse synthetic aperture radar in the presence of phase synchronisation errors. IEEE Trans. on Aerospace and Electronic Systems, 2011, 47(4): 2673–2689.

[6] KONG L J, LI X L, CUI G L, et al. Coherent integration algorithm for a maneuvering target with high-order range migration. IEEE Trans. on Signal Processing, 2015, 63(17): 4474–4486.

[7] WANG Z, YANG W, CHEN Z, et al. A novel adaptive joint time frequency algorithm by the neural network for the ISAR rotational compensation. Remote Sensing, 2018, 10(2): 334.

[8] WU W Z, HU P J, XU S Y, et al. Image registration for InISAR based on joint translational motion compensation. IET Radar, Sonar & Navigation, 2017, 11(10): 1597–1603.

[9] YU X, JIANG R, ZHANG J D, et al. Motion compensation algorithm based on the designing structured gram matrices method. Acta Electronica Sinica, 2014, 8(3): 209–219. (in Chinese)

[10] LING H, WANG Y X, CHEN V C. ISAR image formation and feature extraction using adaptive joint time-frequency processing. Proceedings of SPIE—The International Society for Optical Engineering, 1997, 48(4): 592–603.

[11] DJUROVIC I, THAYAPARAN T, STANKOVIC L. Adaptive local polynomial Fourier transform in ISAR. EURASIP Journal on Advances in Signal Processing, 2006: 036093.

[12] DAI C Y, ZHANG X L, SHI J. Range cell migration correction for bistatic SAR image formation. IEEE Geoscience & Remote Sensing Letters, 2011, 9(1): 124–128.

[13] LU J B, XI Z M, ZHANG M M, et al. Multi-cycle signal processing based on Keystone transform in LFMCW radar. Proc. of the International Conference on Signal Processing Systems, 2010.

[14] DONG Y B, ZHANG H, WANG C, et al. Fine-grained ship classification based on deep residual learning for high-resolution SAR images. Remote Sensing Letters, 2019, 10(11): 1095–1104.

[15] BENGIO Y, LECUN Y. Scaling learning algorithms towards AI. Proc. of the Large-Scale Kernel Machines, 2007: 1−41.

[16] BENGIO Y, COURVILLE A, VINCENT P, et al. Representation learning: a review and new perspectives. IEEE Trans. on Pattern Analysis & Machine Intelligence, 2013, 35(8): 1798–1828.

[17] SMIRNOV E A, TIMOSHENKO D M, ANDRIANOV S N. Comparison of regularization methods for ImageNet classification with deep convolutional neural networks. AASRI Procedia, 2014, 6: 1097–1105.

[18] LI X, LIU G S, NI J L. Autofocusing of ISAR images based on entropy minimization. IEEE Trans. on Aerospace & Electronic Systems, 1999, 35(4): 1240–1252.

[19] ZHANG Y D, DONG Z, CHEN X, et al. Image based fruit category classification by 13-layer deep convolutional neural network and data augmentation. Multimedia Tools & Applications, 2019, 78(3): 3613–3632.

[20] TAN Y L, TANG P J, ZHOU Y M, et al. Photograph aesthetical evaluation and classification with deep convolutional neural networks. Neurocomputing, 2017, 228: 165–175.

[21] RONNEBERGER O, FISCHER P, BROX T. U-net: convolutional networks for biomedical image segmentation. Proc. of the International Conference on Medical Image Computing and Computer-Assisted Intervention, 2015: 234−241.

[22] MCCANN M T, JIN K H, UNSER M. Convolutional neural networks for inverse problems in imaging: a review. IEEE Signal Processing Magazine, 2017, 34(6): 85–95.

[23] PERRY R P, DIPIETRO R C. SAR imaging of moving targets. IEEE Trans. on Aerospace and Electronic Systems, 1999, 35(1): 188–200.

[24] LONG J, SHELHAMER E, DARRELL T. Fully convolutional networks for semantic segmentation. IEEE Trans. on Pattern Analysis and Machine Intelligence, 2015, 39(4): 640–651.
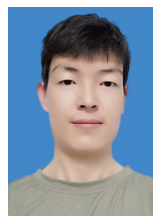
Biographies

SHI Hongyin was born in 1976. He received his Ph.D. degree from Beihang University in 2009. Now, he is a professor in Yanshan University. His main research interests include SAR imaging and moving target detection.
E-mail: shihy@ysu.edu.cn

LIU Yue was born in 1995. She received her B.S. degree from Yanshan University in 2017. Now, she is a master student in School of Information Science and Engineering, Yanshan University. She is mainly engaged in the research of deep learning and ISAR imaging.
E-mail: mlle_liuyue@163.com

GUO Jianwen was born in 1993. He received his B.S. degree from Yanshan University in 2017. Now, he is a master student in School of Information Science and Engineering, Yanshan University. he is mainly engaged in the research of deep learning and ISAR imaging.
E-mail: jianwen_guo@yeah.net

LIU Mingxin was born in 1976. He received his Ph.D. degree from Yanshan University in 2006. He is currently a professor with School of Information Science and Engineering, Yanshan University. His current research interests include stochastic modeling for wireless communication networks and performance valuation for communication system.
E-mail: liumx@ysu.edu.cn